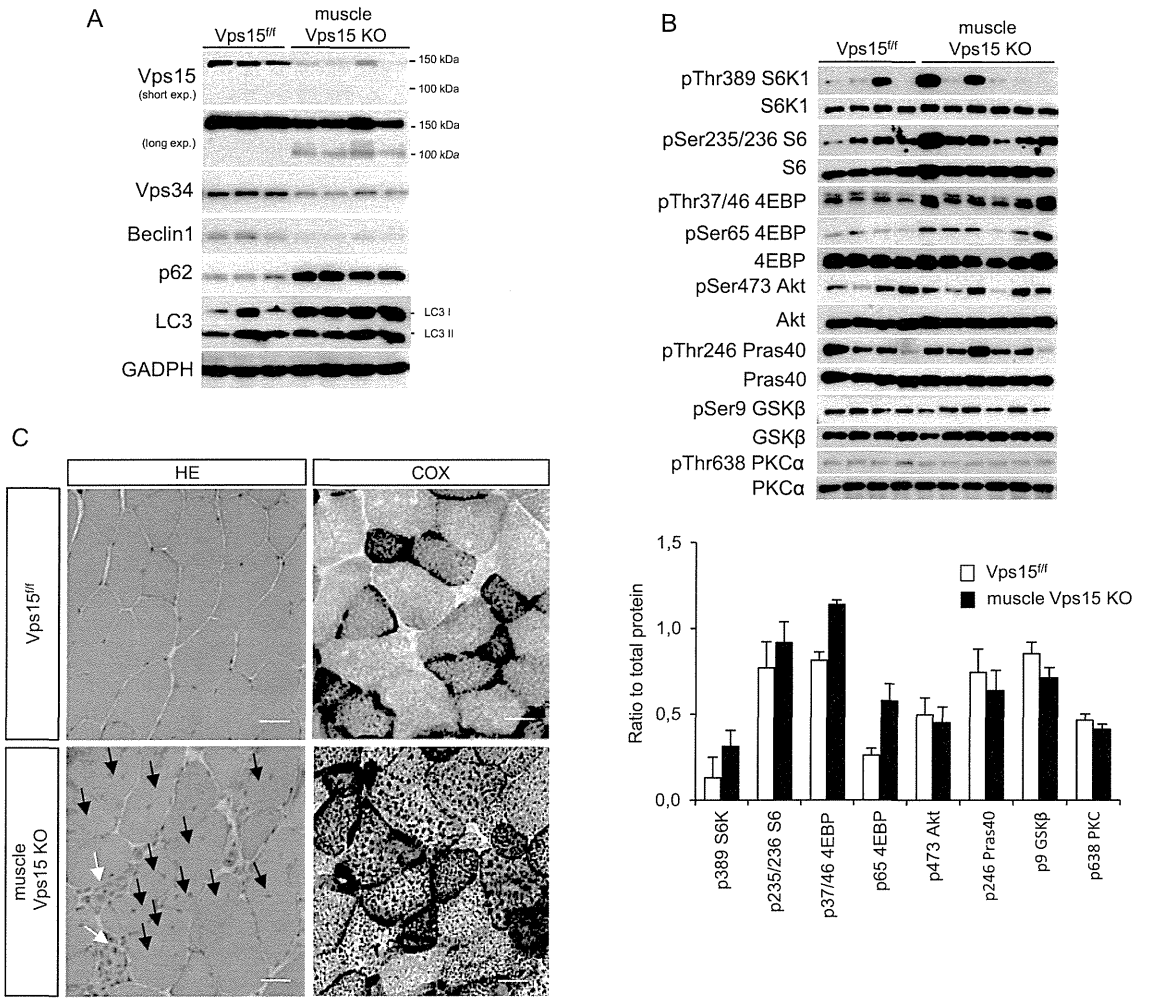

Figure 5. Generation and characterization of muscle-specific*Vps15*-knockout mice.

A. Immunoblot analysis of TA muscle of 2 month old muscle Vps15 KO and matching control mice with indicated antibodies.

B. mTORC1 and mTORC2 activity in TA muscles of 2 month old muscle Vps15 KO and matching control mice analysed by immunoblotting with indicated antibodies. The ratio of phosphorylated to total protein of the densitometric assay is presented. Data are mean ± SEM.

C. Histological analysis of muscles by HE staining and COX activity from 2 month old muscle Vps15 KO and matching control mice. Black arrows indicate centronucleated fibres; white arrows—cell infiltration. Scale bars: 40 μm.

binding protein 1 (4EBP) was observed in Vps15 KO muscles from randomly fed and starved/refed animals (Fig. 5B and Supporting Information Fig. 5). Morphometric examinations did not reveal significant changes in fibre type composition and cross section area in Vps15 KO muscles (Supporting Information Fig. 6A and B). However, severe degenerative changes were evident in the *Vps15*-depleted muscles including appearance of necrotic fibres, cell infiltration, centronucleated fibres as early as 2 months after birth in all types of muscles examined (Fig. 5C, Supporting Information Fig. 6C). The infiltration detected in the *Vps15*-depleted muscles consisted of immune cells, macrophages and T-cells, as revealed by immunostaining with the F4/80 and CD3 markers, respectively (Supporting Information Fig. 7A). Furthermore, the induction of the inflammatory response in *Vps15*-depleted muscles was confirmed at the transcript level by the detection of inflammatory cytokines and cell markers (Supporting Information Fig. 7B). The morphological changes observed in *Vps15*-depleted muscles were accompanied by marked changes in mitochondrial content as assessed by cytochrome c oxidase (COX) assay (Fig. 5C).

Muscle *Vps15* knockout results in autophagy block distinct from *Atg7* knockout

Genetic mouse models carrying muscle specific inactivation of autophagy genes, *Atg7* (Masiero et al, 2009) and *Atg5* (Raben et al, 2008), highlighted the role of macroautophagy in the

maintenance of muscle mass and function. We took advantage of already generated muscle-specific *Atg7* knockout mice (muscle Atg7 KO) and set up a comparative analysis of phenotypes with Vps15 muscle KO (Masiero et al, 2009). For quantitative comparative analysis of *Vps15* and *Atg7* mutants we mainly focused on TA muscles that are predominantly composed by fast twitch fibres and thus relatively homogenous in terms of fibre typing. As shown in Fig. 6A, at the age of 4 months the severity of muscle damage was more pronounced in fast twitch TA muscles from Vps15 KO mice compared to Atg7 KO, as judged by the number of necrotic fibres, centronucleated fibres and cell infiltration. These data point

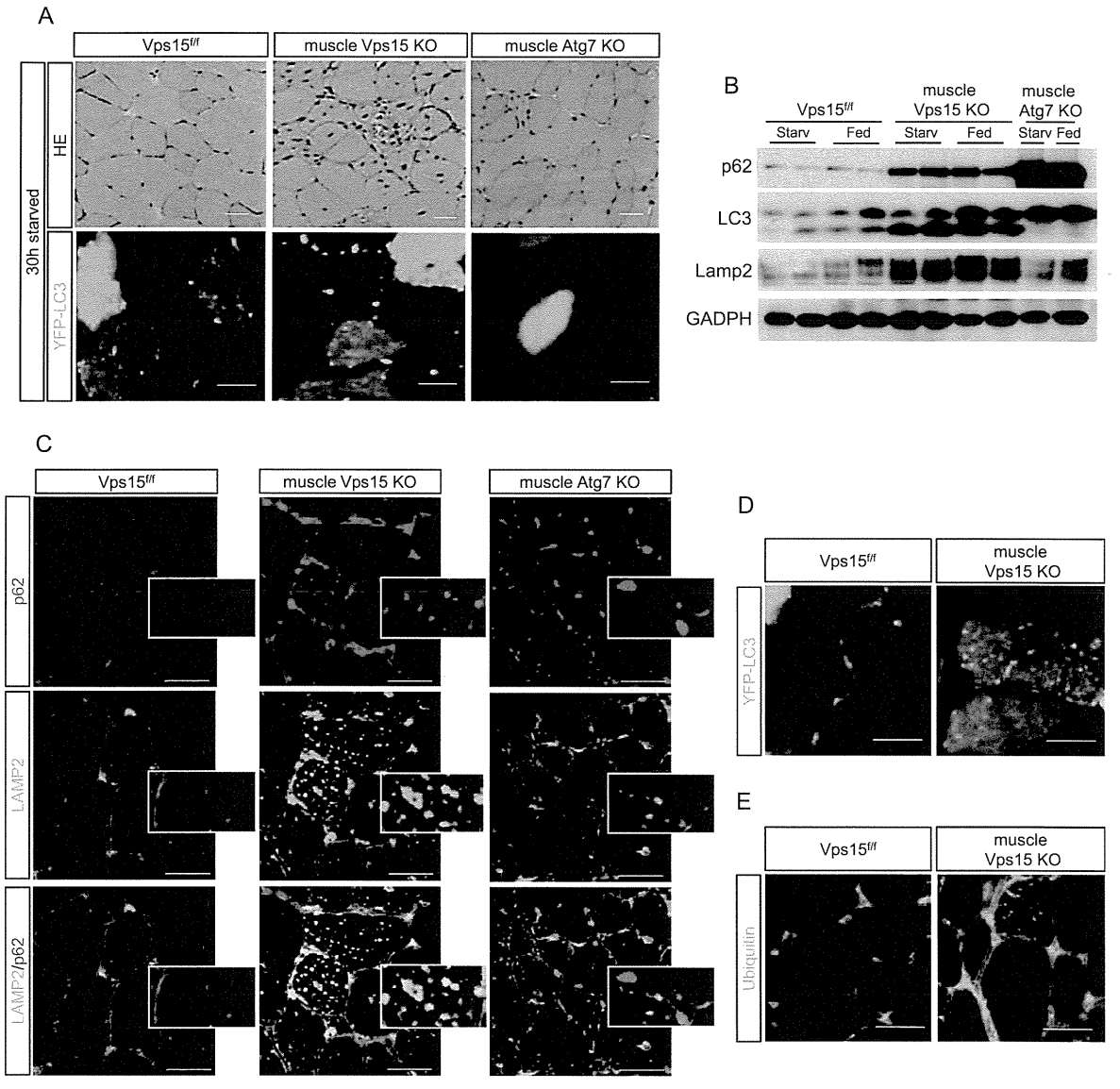

Figure 6. Muscle-specific deletion of *Vps15* is distinct from muscle-specific *Atg7* knockout.

A. Histological analysis of TA muscles of 4 month old 30 h starved muscle Atg7 KO mice, muscle Vps15 KO mice and matching control mice by HE staining and YFP-LC3 fluorescence. Scale bars: 20 μm (HE) and 40 μm (YFP-LC3).

B. Immunoblot analysis of total protein extracts of gastrocnemius muscles with indicated antibodies. Gastrocnemius muscles were dissected from 30 h starved and random fed 4 month old muscle Atg7 KO mice, muscle Vps15 KO mice and matching control mice.

C. Accumulation and co-localization of p62/LAMP2 positive structures in TA muscle of 4 month old random fed muscle Vps15 KO, muscle Atg7 KO and matching control mice. Insets show higher magnification views. Scale bars: 40 μm.

D. Histochemical analysis of TA muscle of randomly fed 4 month old muscle Vps15 KO and matching control mice by LC3-YFP fluorescence. Scale bars: 40 μm.

E. Immunostaining of TA muscle of randomly fed 4 month old Vps15 muscle KO and matching control mice using anti-ubiquitin antibody. Scale bars: 40 μm.

to a broader role of *Vps15* gene in muscle function than the autophagy genes.

After electroporation of TA muscles with YFP-LC3 over-expressing plasmid and after 30 h starvation, Atg7 KO muscles failed to form YFP-LC3 positive autophagosomes, as opposed to starved control mice and muscle Vps15 KO mice (Fig. 6A). Consistently, LC3 was not processed in Atg7 KO mice, whereas Vps15 KO mice displayed an up-regulation of both total and lipidated LC3 as compared to control (Fig. 6B). However, p62 accumulated in both mutants, with higher levels observed in *Atg7*-deficient muscles (Fig. 6B and C). Interestingly, p62 protein appeared differentially localized in Atg7 and Vps15 mutants. While in *Vps15*-deficient TA muscles p62 positive structures were uniformly distributed and largely co-labelled with Lamp2 antibodies representing autolysosomes, in Atg7 mutants p62 was detected in subsarcolemmal protein aggregates void of Lamp2 staining (Fig. 6C). The selective increase in the amount of lysosomes observed in *Vps15*-depleted muscles (Fig. 6C) was confirmed by immunoblot analysis (Fig. 6B) and was unlikely to be due to an induction of lysosomal biogenesis, the expression of the master regulator of lysosome biogenesis TFEB and its downstream targets were unaffected at the transcript level (Supporting Information Fig. 8). In contrast to the control mice, p62 and YFP-LC3 positive structures were evident in muscle Vps15 KO mice that were *ad libitum* fed and did not undergo a starvation protocol (Fig. 6C and D). In addition, *Vps15*-deficient fibres contained high levels of ubiquitinated proteins, as detected by immunostaining (Fig. 6E). To evaluate possible phenotypic differences at early times after gene deletion, we established primary myoblast cultures from $Vps15^{f/f}$ mice, differentiated the myoblasts to myotubes *in vitro* and transduced them with adenoviral Cre to induce gene deletion. In this cell autonomous model we observed that depletion of *Vp15* results in a phenotype similar to the one observed in MEFs as judged by the induction of p62, LC3 and the sparing of mTOR signalling (Supporting Information Fig. 9A and B). Furthermore, by directly comparing *Vps15* and *Atg7* deletion in the myotube cultures we observed that depletion of both genes led to marked accumulation of p62 (Supporting Information Fig. 9C). However, EGFP-LC3 positive puncta were undetectable in *Atg7*-depleted cells even in nutrient-deprived medium, while they were constitutively present in *Vps15*-depleted cells even in nutrient-rich conditions (Supporting Information Fig. 9D). These observations recapitulated data of our *in vivo* Atg7 and Vps15 KO muscles analysis. In conclusion, defects in p62 and ubiquitinated protein degradation in *Vps15*-deficient muscles are accompanied by an up-regulation of LC3 positive autophagosomes and Lamp2 positive lysosomes, which is not observed in *Atg7*-deficient muscles.

Ultrastructural analyses of Vps15 KO muscles

To unquestionably identify the morphological alterations of *Vps15*-deficient tissue, EDL muscles underwent electron microscopy (EM) analysis. As shown in Fig. 7A, *Vps15*-deficient muscles displayed massive accumulation of vacuoles that were frequently found in longitudinal stacks. At higher magnification a large fraction of these vacuoles appeared constituted by variable number of membrane layers (Fig. 7B and C). The various appearance of other vacuoles represented different stages of maturation (*e.g.* lysosomes in Fig. 7D, autophagosome in Fig. 7E). Importantly, autophagosomes, constituted by two layers of membranes enclosing degraded material or organelles (*i.e.* a mitochondrion in Fig. 7E) were frequently observed (Fig. 7E and F). Furthermore, abnormally shaped mitochondria were accumulated and active mitochondria autophagy (mitophagy) was observed (Fig. 7E and G). Thus, EM analysis provided the demonstration that autophagosomes and lysosomes accumulate in *Vps15*-deficient muscles.

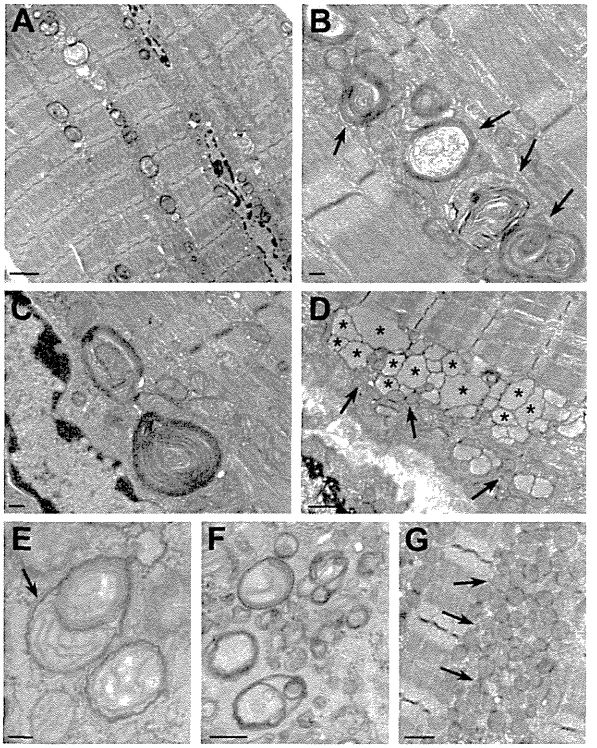

Figure 7. Ultrastructural analysis of *Vps15*-deficient muscles. Electron micrographs of *Vps15*-deficient EDL muscles.

- **A.** Low magnification micrograph showing accumulation along the fibre of numerous autophagic vacuoles of varying morphologies.
- **B.** Enlargement of autophagic vacuoles and vacuoles with lamellated membrane structure (black arrow).
- **C.** Enlargement of a large multilamellar structure in proximity to the nucleus.
- **D.** Accumulation of mitochondria (black arrows) and lysosome like structures (black asterisks).
- **E.** Mitochondria enclosed in an autophagic vacuole (black arrow).
- **F.** Autophagic vacuoles at different stages.
- **G.** Accumulation of mitochondria (black arrows). Scale bars: A and E, 2 μm; B, C and F, 0.2 μm; D and G, 1 μm.

Muscle Vps15 KO mice display symptoms of autophagic vacuolar myopathies

Accumulation of autophagosomes and muscle damage in Vps15 KO mice were reminiscent of AVMs (Nishino, 2003). These are

rare genetic diseases characterized by abnormal lysosomal function. The best characterized AVM is Danon disease, in which the causative gene is *Lamp2* (Nishino et al, 2000). Similarly to *Vps15*-depleted MEFs and muscles, Lamp2 mutant cells are characterized by autophagic build-up, intracellular mistargeting of lysosomal enzymes which is accompanied by increased lysosomal enzyme secretion (Eskelinen et al, 2002). We, therefore, addressed whether muscle Vps15 KO mice displayed distinctive features of AVMs, namely glycogen accumulation and autophagic vacuoles with sarcolemmal features. Analysis of glycogen levels by Periodic acid Schiff (PAS) staining revealed a sharp increase in glycogen accumulation in *Vps15*-deficient muscles as compared to control and *Atg7*-deficient muscles (Fig. 8A). Biochemical analysis confirmed a 60% increase in glycogen levels in Vps15 mutants (Fig. 8B). Using an embedding procedure that allows visualizing glycogen granules as electron-dense small dots, the presence of glycogen was evident in the cytoplasm and inside of both the autophagosomes and the lysosomes by EM (Fig. 8C and Supporting Information Fig. 10). Thus, glycogen is accumulated in Vps15 mutants, distinct to Atg7 mutants.

Presence of the sarcolemmal features is a well-described diagnostic feature of muscles in AVM patients. Proteins which are under normal conditions localized to the membrane (*e.g.* dystrophin, acetylcholinesterase, caveolin 3), are mislocalized and are found inside the affected muscle fibres within the vacuolar structures. Of note, *Vps15*-deficient muscles, but not *Atg7*-deficient muscles, presented with the accumulation of all above-mentioned proteins in the vacuoles within the fibres (Fig. 8D and Supporting Information Fig. 11A). Furthermore, the phenotype of Vps15 muscle KO mice was highly reminiscent of the phenotype observed in muscles of *Lamp2* knockout mice (model of Danon disease) which presented a similar accumulation of glycogen and p62, as well as sarcolemmal features (Supporting Information Fig. 11B). In line with the severe muscle damage in Vps15 muscle KO mice, the levels of plasma creatine kinase were increased by eightfold, another commonly observed symptom in AVM patients (Fig. 8E). To assess the functional consequences of *Vps15* deletion, *in vivo* force measurements on the gastrocnemius muscles were performed in 4 month old mice through stimulation of the sciatic nerve. These analyses showed a significant reduction in absolute force (Fig. 8F), and relative force after normalization to muscle mass (Fig. 8G). Quantitative decrease in muscle force in Vps15 mutants was more prominent as compared to reported in Atg7 mutants (Masiero et al, 2009), and was close to dystrophic mdx mice (Head et al, 1992), indicating a general reduction in force generation and profound muscle weakness.

Class III PI3K overexpression alleviates glycogen accumulation in human AVM muscle cells

As a first step to establish gain-of-function approaches, we asked whether adenoviral mediated overexpression of Vps15 and/or Vps34 in *Vps15*-deficient MEFs was sufficient to rescue the autophagolysosome defects. The overexpression of Vps15 was able to restore the levels of PI3P in the *Vps15*-depleted MEFs, as judged by the localization of 2XFYVE-GFP protein and the measurements of PI3P kinase activity in immunocomplex kinase assays after pull down with antibodies against the Vps15 partners Atg14L and Vps34 (Fig. 9A; Supporting Information Fig. 12A and data not shown). Importantly, as shown in the Fig. 9B and Supporting Information Fig. 12B, the overexpression of Vps15 in *Vps15*-depleted MEFs completely reverted the accumulation of p62 and LC3, indicating an efficient autophagic flux. Interestingly, the overexpression of Vps34 in *Vps15*-deficient cells was not sufficient to rescue the autophagy flux and PIP3s levels, confirming that Vps15 not only regulates Vps34 stability but is also required for PI3K activity (Fig. 9B and Supporting Information Fig. 12B). Importantly, overexpression of the truncated 100 kDa Vps15, unlike the full-length protein, did not further worsen the phenotype of Vps15-mutant cells and was not able to rescue neither PI3P levels nor accumulation of Lamp2, p62, LC3 (Supporting Information Fig. 13A–C).

Next, we asked whether these gain-of-function approaches may be beneficial in human muscle cells from AVM patients (Nishino et al, 2000). Danon disease is caused by point loss-of-function mutations in Lamp2 gene leading to lysosomal storage disease. One prominent clinical feature in these patients is the accumulation of glycogen within the muscle fibres (Malicdan et al, 2008). As shown in Fig. 9C, overexpression of both Vps15 and Vps34 in two different cell lines of Danon disease patients can partially decrease the LC3 levels in these cells. Importantly, this effect was concomitant with a reduction in glycogen accumulation as judged by PAS staining (Fig. 9D). Notably, overexpression of Vps15 alone was not sufficient to improve the

Figure 8. Muscle-specific deletion of *Vps15* manifests with signs of lysosomal storage disease.

A. Deletion of *Vps15* affects glycogen metabolism in muscles. Histological analysis of TA muscles of 4 month old starved muscle Atg7 KO, muscle Vps15 KO and matching control mice by PAS staining to detect glycogen. Scale bars: 40 μm.

B. Glycogen was extracted and levels determined by enzymatic assay in TA muscles of 4 month old randomly fed muscle Vps15 KO and matching control mice. Data are mean ± SEM ($p \leq 0.05$ a: *vs.* $Vps15^{f/f}$).

C. Electron micrographs of *Vps15*-deficient EDL muscle fibre showing accumulation of glycogen granules (black dots) in the cytoplasm, inside the double membrane structures (left) and in lysosome (right). Scale bar: 0.2 μm.

D. Immunostaining of TA muscle of randomly fed 4 month old muscle Atg7 KO mice, muscle Vps15 KO mice and matching control mice using anti-Dystrophin and anti-Caveolin 3 antibodies. Scale bars: 40 μm.

E. Plasma creatine kinase levels of randomly fed 4 month old muscle Vps15 KO and matching control mice. Data are mean ± SEM ($n = 4$–8, $p \leq 0.05$ a: *vs.* $Vps15^{f/f}$).

F. *In vivo* force measurements performed on gastrocnemius muscle of 4 month old muscle Vps15 KO and matching control mice during tetanic contraction. Data are mean ± SEM ($n = 5$ $p \leq 0.05$ a: *vs.* $Vps15^{f/f}$).

G. Relative force measurements after normalization of absolute tetanic force to the gastrocnemius muscle weight. Data are mean ± SEM ($n = 5$ $p \leq 0.05$ a: *vs.* $Vps15^{f/f}$).

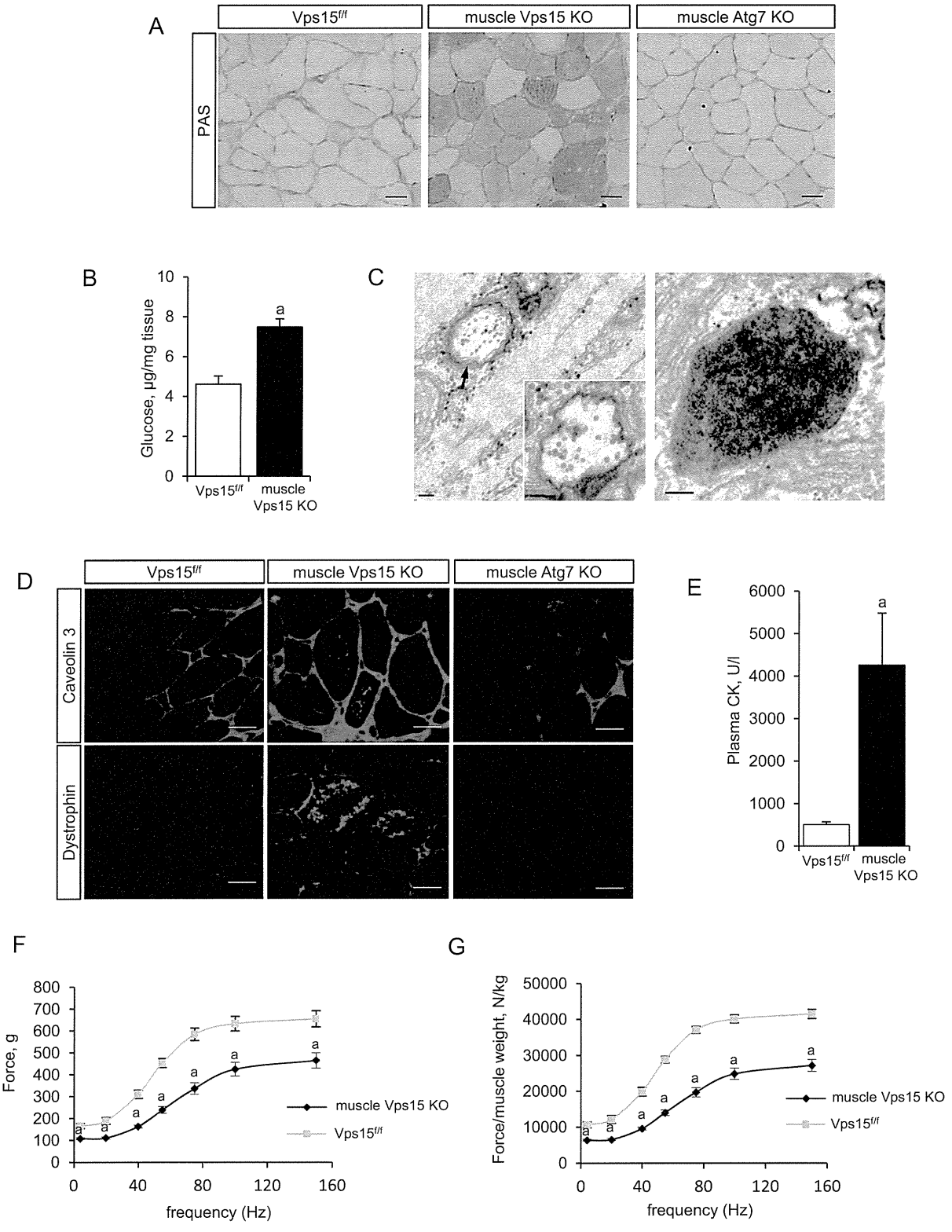

Figure 8.

phenotype of the patient cells, consistent with the data indicating that both Vps15 and Vps34 should be expressed to induce production of PI3P in mammalian cells (Supporting Information Fig. 14A) (Yan et al, 2009). Importantly, overexpression of the truncated 100 kDa Vps15 protein did not affect LC3 or glycogen levels in the patient cells (Supporting Information Fig. 14B and C). Our data are consistent with a critical role of the Vps34/Vps15 complex in regulating autolysosome and endosomal function that are affected in AVMs and other lysosomal storage diseases.

DISCUSSION

To dissect the complex and controversial role of Vps15/Vps34 in autophagy, nutrient sensing and mTOR signal transduction, we generated *Vps15* loss-of-function mutants in MEFs, myotubes and skeletal muscles. While our findings do not support an essential role for Vps15/Vps34 in autophagy initiation and mTOR activation in these cell types, we uncover severe defects in autophagy maturation, lysosomal function, glycogen storage that in skeletal muscles cause AVM with sarcolemmal features, muscle weakness and lysosomal storage disease.

Our data are consistent with a complete loss-of-function of Class III PI3K activity in *Vps15*-mutant cells. Vps15 mutant mice die during early embryonic development before E7.5, similar to the *Vps34* knockout embryos (Zhou et al, 2011). In addition, Cre expression in MEFs leads to a sharp decrease in Vps34 levels few days after *Vps15* excision. This effect is paralleled by a drop in endosomal 2xFYVE-GFP and PI3K kinase activity in Atg14L immunoprecipitates, that is comparable in wortmannin-treated cells and can be rescued by adenoviral transduction of full length Vps15 (Fig. 1C; Fig. 9A and Supporting Information Fig. 12A and 13B). Since the truncated Vps15 protein that is detected after gene targeting, does not form a complex with Vps34 or Beclin 1 and has no effect on mTOR activity and the LC3, p62 or Lamp2 protein levels (Supporting Information Fig. 3B and C), we can conclude that the observed phenotypes are due to Vps15 loss of function. Of note, this Vps15 truncation is sufficient to severely blunt starvation-induced puncta formation for two PI3P-binding proteins regulating autophagy, mCherry-WIPI-1 and the endogenous WIPI-2 (Fig. 2A and B). Our data indicate that the N-terminus domain of Vps15 containing the myristoylation signal for membrane localization and the putative catalytic domain is required to regulate Vps34 stability and PI3K activity, and to maintain cell viability. In addition, we demonstrate that in these cells the Vps15/Vps34 complex is critical for the regulation of PI3P-binding FYVE-domain proteins, ruling out a major role of other PI3K classes or PIP phosphatases.

The implication of Vps15/Vps34 complex in mTOR activation in response to nutrients and in particular to amino acids is extremely controversial. The role of Vps34 as an amino acid availability sensor was proposed using Vps34 and Vps15 knockdown by RNAi in human cells (Byfield et al, 2005; Nobukuni et al, 2005). More recently, it has been proposed that Vps34/Vps15 may mediate the effects of amino acids on mTOR through the stimulation of phospholipase D activity and phosphatidic acid production (Yoon et al, 2011). However, genetic studies in drosophila flies and nematodes did not confirm these observations (Avruch et al, 2009; Juhasz et al, 2008). In $Vps34^{-/-}$ mouse embryos immunostaining of phosphorylated rpS6 was reduced, suggesting a reduced mTORC1 activity (Zhou et al, 2011). However, since the development and viability of $Vps34^{-/-}$ mutants was severely affected, a general reduction in nutrient uptake and sensing, that indirectly leads to the shut-down of the mTOR pathway, should be considered. *In vivo* we do not observe dramatic changes of mTOR signalling in *Vps15*-deficient MEFs and skeletal muscles, as growth factor stimulation is modestly reduced while nutrient stimulation leads to a minor up-regulation (Figs. Fig. 4 and Fig. 5B; Supporting Information Fig. 5). It is conceivable, although unlikely, that the regulation of mTOR activity by Vps34/Vps15 is somehow limited to human cells. Alternatively, the effects of Vps34/Vps15 on mTOR may not be direct, but secondary consequences of cellular responses to the disruption of the Vps34/Vps15 complex. Interestingly, lysosomes and p62 levels are involved in upstream regulation of mTOR activity (Duran et al, 2011; Zoncu et al, 2011), and both components are dramatically increased in Vps15 mutant cells (Fig. 2D and F; Fig. 3B; Fig. 6B and C). Similarly, recent data on conditional *Vps34* knockout mice in liver and heart (Jaber et al, 2012) indicated that the steady-state level of mTOR signalling was not affected in *Vps34*-null MEFs, liver or cardiomyocytes. However, contrary to our observations, amino acid-stimulated mTOR activation was suppressed in the absence of Vps34 *in vitro* in immortalised MEF cultures. One possible explanation for this discrepancy is that we used primary cultures of MEFs to assess the status of mTOR signalling in response to both amino

Figure 9. Overexpression of Vps15/Vps34 complex rescues autophagy defects in *Vps15*-depleted MEFs and upregulates autophagy in primary myotube cultures from Danon disease patients improving the glycogen metabolism.

A. Intact Vps15 is required for Vps34 kinase activity. Beclin 1 complexes were immuno-purified with antibody against ATG14L from *Vps15*-depleted MEFs, *Vps15*-depleted MEFs transduced with indicated adenoviral vectors or from control MEFs in which Vps34 was pharmacologicaly inactivated. Activity of Vps34 complexes was assayed by an *in vitro* kinase assay with phosphatidylinositol and ^{32}P-ATP as substrates. ^{32}P-PI3P was resolved by thin layer chromatography and visualized by autoradiography. Fractions of the kinase reaction were used for immunoblotting for Beclin 1.

B. *Vps15*-depleted MEFs were transduced with indicated adenoviral vectors, cells collected 60 h post-infection and total protein extracts immunobloted with indicated antibodies. The ratio of p62 or LC3 to GAPDH of the densitometric assay is presented.

C. Human myoblasts derived from Danon disease patients were differentiated to myotubes and then transduced 2 days post-differentiation with indicated adenoviral vectors. Cells were collected 3 days post-infection and total protein extracts were analysed by immunoblotting with indicated antibodies. The ratio of LC3 to GAPDH of the densitometric assay is presented.

D. PAS staining of the glycogen in human myotubes derived from Danon disease patients with and without Vps15 and Vps34 overexpression, analysed 3 days post-infection. Scale bars: 20 μm.

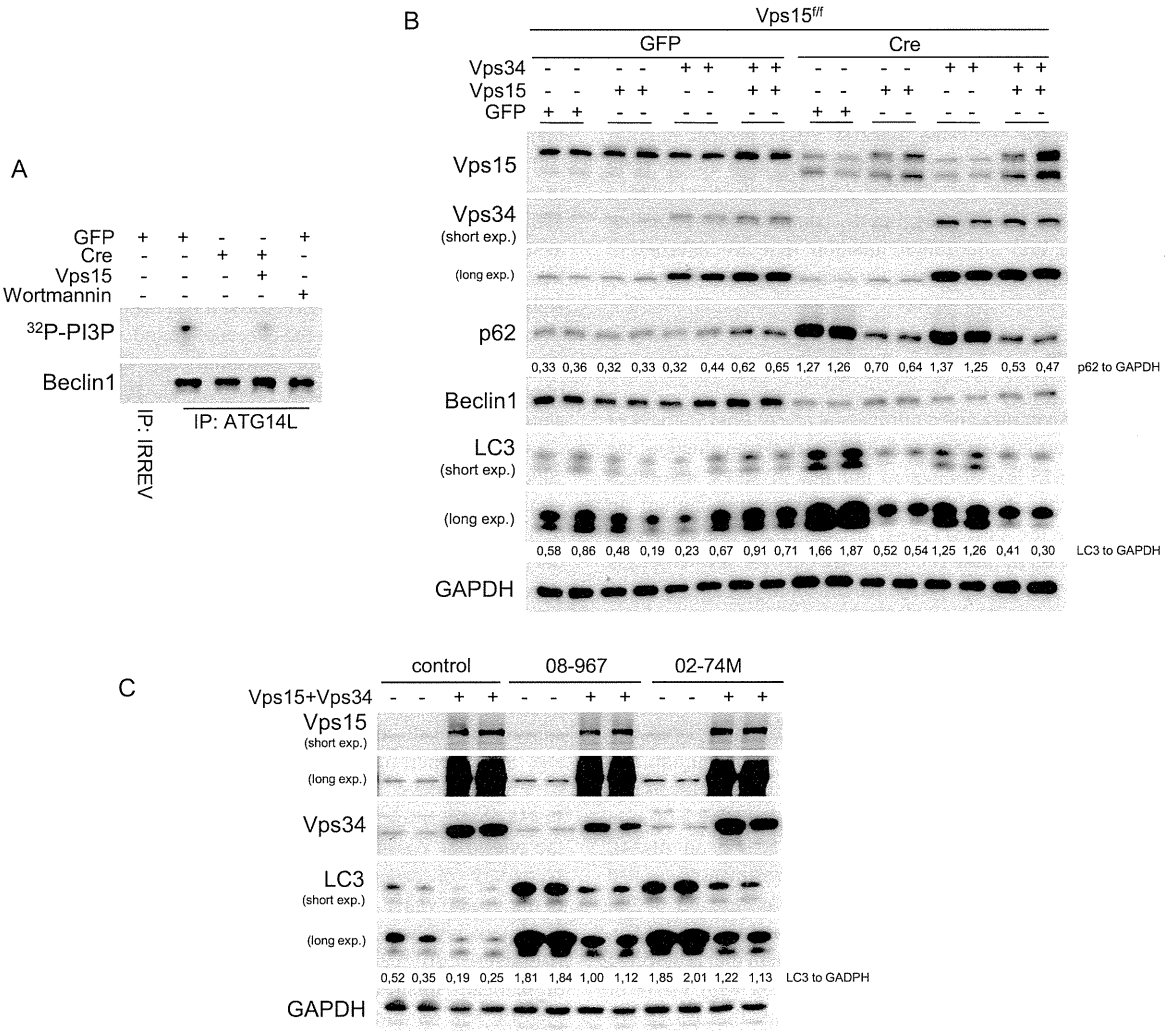

Figure 9.

acids and dialysed foetal calf serum. Moreover, we addressed the dynamics of mTOR activation by both stimuli in time course experiments. Finally, we measured wortmannin sensitivity and showed similar sensitivity of control and *Vps15* mutant cells to the PI3K inhibitor, suggesting that additional PI3K classes mediate mTOR activation by amino acids. However, we cannot exclude that *Vps34* deletion causes effects on mTOR signalling that are not mimicked by *Vps15* deficiency.

Different Vps15/Vps34 complexes are involved in multiple steps of autophagosome formation and endosomal trafficking. A complex also containing Beclin 1 and ATG14L promotes autophagosome formation during the early nucleation step, at least in part through the recruitment of the PI3P binding effectors WD repeat domain phosphoinositide-interacting (WIPI) proteins at the phagophore assembly sites (Matsunaga et al, 2009). Moreover, a distinct Vps15/Vps34 complex containing Beclin 1 and UVRAG, and localized at the endosomes, regulates autophagosome maturation by favouring fusion with lysosomes/late endosomes and endocytic trafficking (Zhong et al, 2009). In Vps15 mutant MEFs and skeletal muscles we still detect autophagosome formation as indicated by endogenous LC3 lipidation and puncta formation after LC3-GFP ectopic expression (Fig. 2C, D and E; Fig. 3A and B; Fig. 5A, Fig. 6A, B and D). More importantly, EM of skeletal muscles undoubtedly reveals the accumulation of double membranated autophagosomes containing mitochondria, glycogen and cytosolic components in Vps15 mutant tissue (Figs. Fig. 7 and Fig. 8C; Supporting Information Fig. 10). Our data are consistent with recent analysis of *Vps34*-deficient sensory neurons and lymphocytes reporting defects in the endosomal pathway but not in autophagosome formation (McLeod et al, 2011; Zhou et al, 2011), while they contrast with the reported defects of autophagy initiation in *Vps34*-deficient liver and heart (Jaber et al, 2012). It is possible that in different cell types and physiological conditions, the Vps15/Vps34/Beclin1/ATG14L complex is dispensable for autophagosome nucleation. Interestingly, there is increasing evidence of non-canonical routes to autophagy that can bypass this complex and WIPI-1/2 effectors (Codogno et al, 2011). Conversely, we trace a block in the late phases of the autophagic flux by the following experimental evidences: (i) immunostaining or immunoblot analysis of p62, ubiquitin and lysosomal marker Lamp2, indicating that ubiquitinated cargo proteins are not properly digested after p62-mediated delivery to the lysosomes (Fig. 2D, E and G); (ii) lack of red puncta induction in Vps15 mutant MEFs after ectopic expression of mRFP-EGFP tandem fluorescent-tagged LC3 reporter protein, consistent with an alteration in acidic pH or hydrolase content that does not efficiently quench the EGFP signal (Fig. 3A); (iii) flux experiment with lysosomal inhibitors, showing that mutant cells mimic the effect of bafilomycin A1 on LC3 processing (Fig. 3B and Supporting Information Fig. 3A); (iv) processing defects of GST-BHMT fusion reporter protein at the autolysosome step (Fig. 3C); (v) decreased activity of lysosomal enzymes and sorting defects leading to the excretion to the enzymes to the extracellular fluid (Fig. 3D). These defects in the autolysosomal function suggest that Vps15/Vps34 complexes containing UVRAG or additional partners are impaired by the *Vps15* deletion and are not functionally compensated. Notably, there is growing evidence highlighting the important role of PI3P in the autophagosome maturation. For instance, reduction of cellular PI3P levels by overexpression of PI3P phosphatase MTMR3 results in decreased size of autophagosomes suggesting a role for PI3P in autophagosome maturation (Taguchi-Atarashi et al, 2010). Recently, the essential direct role of TECPR1 protein in autophagosome maturation has been demonstrated (Chen et al, 2012). TECPR1 is a binding partner of Atg5/Atg12 complex which requires PI3P for its function on complex recruitment to autolysosomes. Strikingly, depletion of TECPR1 phenocopies the deletion of *Vps15* in terms of p62 and LC3 accumulation while autophagosome formation is preserved. Since *Vps15*-depleted cells have decreased levels of PI3P, it is tempting to speculate that PI3P are indispensable for autophagosome maturation by acting on target proteins such as TECPR1.

Consistently, the phenotype of *Vps15*-deficient skeletal muscles differs from the Atg7 mutants (Fig. 6; Fig. 8; Supporting Information Fig. 9C and D). In contrast to the Vps15 mutants, *Atg7* deletion impairs LC3 lipidation, autophagosome formation and mitophagy. However, *Atg7* deletion does not cause accumulation of glycogen and sarcolemmal features within the fibres that are observed in the Vps15 mutants. Interestingly, dysfunctional Endosomal Sorting Complex Required for Transport (ESCRT) leads to defects similar to the *Vps15* deletion. The ESCRT machinery consists of four protein complexes, named ESCRT-0, -I, -II, -III, that are involved in sorting of ubiquitinated cargoes and in multivesicular endosome biogenesis (Rusten et al, 2012). Depletion of ESCRT subunits causes autophagosome accumulation and defects in receptor tyrosine kinase recycling (Lee et al, 2007; Rusten et al, 2007), adding new evidence that defects in late endosomal/lysosomal functions may be responsible of the Vps15 mutant phenotype. Whether the autophagosome build-up observed in lysosomal storage disease and ESCRT deficiency is a cause or a compensatory response of the disease state is still an open question. Inhibition of autophagy by Atg5 and Atg7 knockdown delays neuronal cell loss caused by dysfunctional ESCRT-III (Lee and Gao, 2009). However, in an animal model of lysosomal storage Pompe disease due to GAA deficiency, the combined deletion of Atg5 worsens the myopathy, though permitting successful enzyme replacement therapy in autophagy deficient skeletal muscles (Raben et al, 2008; Raben et al, 2010). It will be important to determine whether the myopathy in Vps15 mutants is affected by altering the autophagosome formation.

AVMs are rare disorders including Danon disease and X-linked myopathy with excessive autophagy (XMEA), infantile AVM, adult-onset AVM with multi-organ involvement, X-linked congenital AVM (Nishino, 2003). The only known causative gene is *Lamp2* whose mutations cause Danon disease. In addition, lysosomal storage diseases are metabolic disorders that are often, but not exclusively, due to mutations in genes encoding lysosomal degrading enzymes, leading to defects in lysosomal function (Eskelinen and Saftig, 2009). Individually, AVMs and lysosomal storage diseases occur with incidences of

less than 1:100,000. However, as a group the incidence is about 1:5000–1:10,000 (Fuller et al, 2006). Interestingly, in both AVMs and lysosomal storage diseases the accumulation of autophagosomes, glycogen and sarcolemmal features are pathognomonic morphological hallmark of the disease. We show that *Vps15* loss-of-function mouse mutants recapitulate these features of the disease (Fig. 5; Fig. 6; Fig. 7; Fig. 8), while Vps15/Vps34 gain-of-function approaches in human muscle cells from Danon patients alleviate LC3 and glycogen accumulation (Fig. 9C and D). Although future work will tell whether mutations in the Class III PI3K pathway underlie a fraction of human AVM, our study unquestionably demonstrates that the modulation of Vps15/Vps34 expression has a direct functional role in the development of AVM.

MATERIALS AND METHODS

Generation of Vps15$^{f/f}$ mice

The Vps15 conditional mutant mouse line was established at the MCI/ICS (Mouse Clinical Institute – Institute Clinique de la Souris, Illkirch, France). The targeting vector was constructed as follows. The 5′ (4.2 kb), 3′ (3.5 kb) and inter-loxP (1.4 kb) fragments were PCR amplified on a 129 BAC DNA (reference bMQ366b03) and sequentially subcloned into an MCI proprietary vector containing the LoxP sites and a Neo cassette flanked by Flippase Recognition Target (FRT) sites. The linearized construct was electroporated in 129S2/SvPas mouse embryonic stem (ES) cells. After selection, targeted clones were identified by PCR using external primers and further confirmed by Southern blot with 5′ and 3′ external probes. Two positive ES clones were injected into C57BL/6J blastocysts, and derived male chimaeras gave germline transmission. The excision of the neomycin-resistance cassette was performed *in vivo* by breeding the chimeras with a Flp deleter line (C57BL/6N genetic background). The Flp transgene was segregated by breeding the first germ line mice with a wild type C57BL/6N animal. For generation of whole body or muscle specific *Vps15* knockout, Vps15 floxed mice were crossed with transgenic mice expressing Cre recombinase under the control of a CMV promoter or Human Skeletal Actin promoter, respectively (Miniou et al, 1999; Schwenk et al, 1995). Genomic DNA isolated from mouse tail snip or tissues was analysed by PCR. Cre-mediated recombination was confirmed by PCR with genomic DNA from muscles. The following PCR primers were used:

EF 5′-GCTAGGCCCTCTTAGACGGTTTCAGAC-3′;
ER 5′-AGCTGTGTGCTTCTGTAGCAGCAACTG-3′;
LF 5′-GACCGAGGCATACGGTACTTTTACG-3′;
LR 5′-ACGTCATGTCATTCTTTCCAGCCGC-3′.

The following combinations of the primers were used: to check presence of distal loxP sites—LF/LR; to check Cre mediated excision of the locus—LF/ER; to check Flp mediated excision of Neomycin cassette—EF/ER. The primers used for Cre recombinase are: 5′-GCGGTCTGGCAGTAAAAACTATC-3′ and 5′-GTGAAACAGCATTGCTGTCACTT-3′. All animal studies were approved by the Direction Départementale des Services Vétérinaires, Préfecture de Police, Paris, France (authorization number 75-1313).

Knockout mice and *in vivo* transfection experiments

Muscle specific *Atg7* knockout mice were described previously (Masiero et al, 2009). *In vivo* transfection experiments were performed by intramuscular injection of plasmid DNA in TA muscle followed by electroporation as described (Mammucari et al, 2007). Muscles were collected 10 days after electroporation and frozen in liquid nitrogen for subsequent analyses. Cryosections of TA muscles expressing YFP-LC3 were examined in a fluorescence microscope as described (Mizushima et al, 2004). Lamp2 knockout mice were described previously (Tanaka et al, 2000).

Reagents

The following primary antibodies were used: anti-Vps15 antibody and anti-p62 (SQSTM) (Abnova), anti-LAMP2 and anti-LAMP1 (Abcam), anti-Acetylcholinesterase (Novus), anti-Dystrophin (Novocastra), anti-WIPI-2 (Abgent), anti-Atg14L (MBL). All other antibodies were from Cell Signalling. 2xFYVE-GFP expressing vector was kindly provided by Sharon Tooze. EGFP-LC3 adenovirus was a kind gift of Aviva Tolkovsky (49), tfLC3 adenovirus was a kind gift from Junichi Sadoshima (Hariharan et al, 2010). The human WIPI-1 cDNA was subcloned from pEGFP.C1-WIPI-1 (Proikas-Cezanne et al, 2004) into EcoRI/XhoI of mCherry (kindly provided by Roland Brock). GST-BHMT construct was a kind gift from Carol Mercer (Dennis et al, 2009). Vps15, Vps34 and ΔVps15(293-1358 aa) adenoviruses were generated by Vector BioLabs (USA). Wortmannin and bafilomycin A1 were from Sigma.

Cell cultures

Vps15$^{f/f}$ MEFs were prepared from embryos at embryonic day 13.5 as previously described (Shima et al, 1998). Briefly, embryos were minced and incubated in 0.25% trypsin at 37°C for 15 min, then passed through a cell strainer (Falcon). Dulbecco's modified Eagle's medium (DMEM), containing 10% of fetal calf serum (FCS) was added to the cell suspension. Cells were then centrifuged at 1000 rpm and the pellet was suspended in DMEM containing 10% FCS. To obtain Vps15$^{-/-}$MEFs, fibroblasts were transduced at 50 MOI by adenoviruses Cre-GFP or GFP as a control and incubated for 3 days before analyses.

For LC3 analyses MEFs were transduced with LC3 adenoviruses (EGFP-LC3 or tfLC3) 48 h after CAG-Cre adenovirus transduction. For FYVE domain and WIPI-1 analyses MEFs were transfected with 2xFYVE-GFP or mCherry-WIPI-1 using Lipofectamine 2000 reagent as recommended by manufacturer (Invitrogen).

For growth factor or amino acid treatment experiments MEFs were first starved for 18 h in serum-free medium and then additionally for 2 h in EBSS. Cells were then stimulated for indicated time with dialysed Fetal bovine serum (FBS) (final concentration 10%) or stimulated with amino acid mixture. After stimulation, the final concentration of amino acids in the media was the same as in DMEM. The 10× amino acid mixture was prepared from individual amino acid powders.

GST-BHMT assay was performed as described previously (Dennis et al, 2009).

Primary myoblast cultures were obtained from gastrocnemius and TA muscles of 4-week-old mice, as described (Aguilar et al, 2007). Briefly, muscles were digested with five sequential 10-min incubations in DMEM/HamF12 medium containing 0.14% pronase (Sigma). The supernatants from the second, third and fourth digestions were pooled and filtered through a 100 μm cell strainer. Cells were centrifuged, washed twice, counted and plated at low density (100 cells/cm^2) on

12-well plates coated with gelatin (Type A from pig skin; Sigma). Cells were grown in medium composed of DMEM/Ham F12, 2% Ultroser G (Biosepra), 20% FCS, penicillin, streptomycin and L-glutamine. After 1 week, wells containing myoblasts without contamination with fibroblasts were trypsinized, pooled and expanded. For the experiments, myoblasts were differentiated to myotubes in DMEM/Ham's F12 medium supplemented with 2% horse serum. At day 2 of differentiation myotubes were transduced by Cre adenovirus at 5MOI and incubated for another 3 days for immunoblot analyses and 2 days before transduction with EGFP-LC3 adenovirus. The subcellular distribution of EGFP-LC3 was analysed 24 h post-infection by fluorescent microscopy.

In rescue experiments *Vps15*-deleted and control MEFs were infected with GFP, Vps15, Vps34 or ΔVps15 adenoviruses at 200 MOI and analysed 60 h after.

Human primary myoblasts were established from muscle obtained from biceps brachii (Nishino et al, 2000). Genetic mutations were identified for 02-74M (Danon disease) LAMP2 c.928G > A and for 08-967 (Danon disease) LAMP2 c.371_372del. Cells were grown and differentiated similarly to mouse myoblasts. Two days after differentiation cells were transduced by GFP, Vps15, Vps34 or ΔVps15 adenoviruses at 150 MOI. Three days post-infection cells were analysed by immunoblot or stained with PAS to visualize glycogen.

Metabolic studies in mice

At two months of age, a GTT was performed in mice after an overnight fasting (14 h). Mice were intraperitoneally injected with 2 g/kg glucose, and blood was collected from the tail vein for determination of glucose levels at 0, 15, 30, 45 and 100 min by Glucotrend glucometer (Roche Diagnostics). ITT was performed at two months of age. Overnight fasted mice were intraperitoneally injected with 1 U/kg insulin (Actrapid) and the glucose concentration in whole blood from the tail vein was measured at 0, 15, 30 and 60 min.

Histology

Soleus, EDL and TA muscles of male mice were embedded in Cryo-Gel (Electro Microscopy Sciences), frozen in isopentane pre-chilled in liquid nitrogen and stored at −80°C. Transverse 6 μm thick cross sections were collected along the entire length of the muscle at 300 μm intervals with a cryostat (Leica CM 1850) and stained with haematoxylin/eosin solution, PAS or assayed for COX activity.

Microscopy

For confocal microscopy cells were grown on coverslips, fixed with 4% paraformaldehyde in PBS and permeabilized with 0.2% TritonX100 in PBS for 5 min, followed by blocking in 3% BSA in PBS. Slides were then treated with primary antibodies overnight. Secondary antibodies used for this assay were anti-rat IgG Alexa Fluor 488 and anti-mouse IgG Alexa Fluor 555 (Invitrogen). Confocal images were acquired with an optical slice of 0.8 μm using a 40×/0.75 oil immersion objective using LSM 700 confocal microscope (Zeiss) and analysed using ZEN software (Zeiss).

Fluorescence and light microscopy were performed using an inverted microscope (Eclipse Ti-S; Nikon) and 10×/0.30, 20×/0.50 or 40×/0.785 Plan Fluor objectives (Nikon). Images were captured using a Super high-definition cooled colour camera head DS-Ri1 (Nikon) and NIS Elements software (Nikon). All samples for microscopy were viewed at room temperature.

Direct fluorescence of mCherry-WIPI-1 and indirect immunofluorescence of endogenous WIPI-2 was conducted as previously described (Proikas-Cezanne et al, 2004; Proikas-Cezanne and Pfisterer, 2009). Z-stacks (optical sections of 0.5 μm) were acquired using Zeiss/Axiovert 100M/LSM510 and a 63 × 1.4 DIC Plan-apochromat objective, and projections of individual optical sections were used to generate final images. mCherry-WIPI-1 puncta formation was assessed as previously described (Proikas-Cezanne et al, 2007).

Protein extraction, immunoblotting and immunoprecipitation

For immunoblot analysis, cells were washed twice with cold phosphate-buffered saline (PBS), scraped off of the culture dish in lysis buffer B containing 50 mM Tris (pH 8.0), 1% NP-40, 120 mM NaCl, 20 mM NaF, 1× protease inhibitors (Roche), 1× PhosphoStop Inhibitors (Roche). Protein extract from muscle tissue was prepared in 20 mM Tris-HCl (pH 8.0), 5% glycerol, 138 mM NaCl, 2.7 mM KCl, 1% NP-40, 20 mM NaF, 5 mM EDTA, 1× protease inhibitors (Roche), 1× PhosphoStop Inhibitors (Roche). Homogenates were spun at 12,000×*g* for 10 min at 4°C. Protein extracts were resolved by SDS-PAGE before transfer onto PVDF membrane and incubation with the primary antibodies. For immunoprecipitations, the indicated antibodies were added to the cell extracts and incubated at 4°C for 2 h. The complexes were pulled down by incubating at 4°C for additional 1 h with protein G-sepharose (GE Healthcare). The resulting beads were washed with lysis buffer five times and complexes eluted by boiling in sample buffer before proceeding with immunoblot analysis.

Real-time quantitative PCR

Total RNA was isolated using RNAeasy Mini Kit (QIAGEN), single-strand cDNA was synthesized from 1 μg of total RNA with random hexamer primers and SuperScript II (Invitrogen). Real-time quantitative PCR (RTqPCR) was performed on MX3005P instrument (Agilent) using a Brilliant II SYBR Green QPCR Low ROX Master Mix (Agilent). The relative amounts of the mRNAs studied were determined by means of the $2^{-\Delta\Delta CT}$ method, with pinin as a reference gene and control treatment or genotype as the invariant control. Pairs of primers were used in the study: *Vps15* exon 2 CCTGGTGGTTGTGAAGGTCT and AGCGCTTCTCGATGTTGTTT, *Vps15* exon 4 TTGTCCTGGTGTCCGTGATA and GAGTGTCCTCAGGGCTTCAG, TNF-α CAAGGGACAAGGCTGCCCCG and GCAGGGGCTCTTGACGGCAG, IL6 TAGTCCTTCCTACCCCAATTTCC and TTGGTCCTTAGCCACTCCTTC, IL1β CTGGTGTGTGACGTTCCCATTA and CCGACAGCACGAGGCTTT, F4/80 CCCCAGTGTCCTTACAGAGTG and GTGCCCAGAGTGGATGTCT. For analyses of TFEB and its targets transcript levels, primer sequences were taken from (Pena-Llopis et al, 2011).

Biochemical assays

For glycogen content, frozen tissue samples were powdered in liquid nitrogen. The powder was used for enzymatic analysis of glycogen after perchloric acid extraction (Bergmeyer and Bernt, 1974). For creatine kinase assay, blood samples were taken by peri-orbital bleeding in random-fed mice. Activity of creatine kinase in plasma was determined with a multiparametric automate (Olympus AU 400) by colorometric density.

Lysosomal enzyme activities were measured using fluorometric assays. Cell lysates were prepared in water by repetitive freezing-defrosting cycles. Then 20 μL of cell culture media or 3 μg of total protein extract

The paper explained

PROBLEM:

Autophagy plays an important role in tissue homeostasis and renewal through the isolation of cellular components and their disposal in lysosomes. The relevance for skeletal muscle function is underlined by the observation that a variety of human myopathies are accompanied by a deregulation of autophagic flux. The Vps15/Vps34 complex has Class III PI3 kinase activity. Genetic studies in yeast have demonstrated the Vps15/Vps34 requirement for endosomal sorting and autophagy. However, the pathophysiological impact of these gene products in mammalian tissues, including skeletal muscle, remains unclear and is the object of our investigation.

RESULTS:

Vps15 loss-of-function mutants in skeletal muscles recapitulate a disease condition of AVM, characterized by profound muscle weakness and the accumulation of autophagosomes, glycogen and sarcolemmal features within the muscle fibres. Conversely, the overexpression of Vps15 and Vps34 in human muscle cells from Danon patients suffering of AVM alleviates metabolic disturbances.

IMPACT:

We have characterized *in vivo* the steps in autophagosome formation and endosomal trafficking that require Class III PI3K activity in mammalian cells. Our findings in human patient cells and animal model open the possibility that the modulation of Vps15/Vps34 signalling has an important functional role in the development of AVMs and lysosomal storage diseases. Finally, strategies ameliorating Vps15/Vps34 functions may be beneficial for this broad class of metabolic diseases.

were incubated at 37°C with 0.1 mL of 0.1 M sodium citrate, pH 4.6 containing the corresponding 4-methylumbelliferyl substrate (3 mM). The reaction was stopped with 0.1 mL 0.2 M glycine, pH 10.4, and the 4-methylumbelliferyl fluorescence was measured using fluorometric plate reader.

Electron microscopy

EDL muscles were dissected from $Vps15^{f/f}$ and HSA-Cre^{+};$Vps15^{f/f}$ mice. Muscles were fixed at RT in 3.5% glutaraldehyde in 0.1 M sodium cacodylate buffer (pH 7.4) for 2 h and kept in fixative before further use. In standard embedding preparations, small bundles of fixed fibres were post-fixed in 2% OsO_4 in 0.1 M sodium cacodylate buffer for 2 h and block-stained in aqueous saturated uranyl acetate. For glycogen analysis, small bundles of fixed fibres were post-fixed in 0.5% OsO_4-1.5% $Fe(CN)_6$. Specimens from both procedures, after dehydration, were embedded in an epoxy resin (Epon 812). After staining with Toluidine Blue dye, the sections were viewed on a Leica DMLB fluorescence microscope (Leica Microsystem). For EM, ultrathin sections (50 nm) were cut and, after staining in 4% uranyl acetate and lead citrate, examined with a Morgagni Series 268D electron microscope (FEI Company), equipped with Megaview III digital camera.

In vitro Vps34 lipid kinase assay

Immuno-purified complexes were washed in 1× kinase base buffer (KBB) consisting 20 mM HEPES pH 7.4, 1 mM EGTA, 0.4 mM EDTA, 5 mM $MgCl_2$. Half of the volume was taken for input, the remainder was centrifuged and excess 1× KBB was removed. 40 μL of 1× kinase assay buffer was added to precipitated kinase (1×KBB supplemented with 0.1 mg/mL phosphatidylinositol, 50 μM cold ATP, 5 μCi ^{32}P-ATP, 5 mM $MnCl_2$ and 50 μM DTT) followed by incubation at 37°C for 30 min with vigorous shaking. Reaction was quenched by addition of 1 M HCl, followed by lipid extraction with two volumes of MeOH:$CHCl_3$ (1:1). Organic phase was resolved by thin layer chromatography (Whatman). Resolution of phospho-lipids was achieved using a buffer composition of CHCl:MeOH(99%):NH_4OH(30%):water (129:100:4.29:24). Resolved plates were analysed by autoradiography. Vps34 was pharmacologicaly inhibited by addition of 50 nM Wortmannin in cell culture and kinase reaction buffer.

Statistical analysis

A two-tailed Student's *t*-test was used for statistical analysis. All data are expressed as means ± SEM, and significance was established at the $p \leq 0.05$ level.

Author contributions

INe and GP designed, performed most of the experimental work and analysed data. BB performed muscle force measurement experiments. CP and FP performed EM experiments. AM and TPC performed experiments with WIPI-2 and WIPI-1. RCR in KLG lab performed *in vitro* PI3P kinase assay. CC lab performed lysosomal enzymes assays. INi shared reagents and expertise. MS provided mouse muscle Atg7 KO line and performed muscle electroporation experiments. MP conceived and directed the study. MP, INe and GP wrote the manuscript. All authors discussed the results and commented on the manuscript.

Acknowledgements

We are grateful to the members of INSERM-U845 for support, and to Patrice Codogno, Sharon Tooze, Paul Saftig, Patrick Dennis, Aviva Tolkowsky and Junichi Sadoshima for helpful discussions and sharing reagents. We thank Sophie Berissi, Delphine Pion, Jean-Philippe Puech, Frank Ling and Sylvie Fabrega for excellent technical support. The mouse mutant line was established at the Mouse Clinical Institute (Institute Clinique de la Souris, MCI/ICS) in the Genetic Engineering and Model Validation Department. This work was supported by grants from DFG, SFB 773 to TP-C,

Research Grant # GGP08153 from the Italian Telethon ONLUS Foundation to FP and from the European 7th Framework MyoAge program, from the European Research Council, from Fondation de la Recherche Medicale (DEQ20061107956) and from Fondation Schlumberger pour l'Education et la Recherche to MP.

Supporting Information is available at EMBO Molecular Medicine Online

The authors declare that they have no conflict of interest.

References

Aguilar V, Alliouachene S, Sotiropoulos A, Sobering A, Athea Y, Djouadi F, Miraux S, Thiaudiere E, Foretz M, Viollet B, *et al* (2007) S6 kinase deletion suppresses muscle growth adaptations to nutrient availability by activating AMP kinase. Cell Metab 5: 476-487

Avruch J, Long X, Ortiz-Vega S, Rapley J, Papageorgiou A, Dai N (2009) Amino acid regulation of TOR complex 1. Am J Physiol Endocrinol Metab 296: E592-E602

Banta LM, Robinson JS, Klionsky DJ, Emr SD (1988) Organelle assembly in yeast: characterization of yeast mutants defective in vacuolar biogenesis and protein sorting. J Cell Biol 107: 1369-1383

Beggs AH, Bohm J, Snead E, Kozlowski M, Maurer M, Minor K, Childers MK, Taylor SM, Hitte C, Mickelson JR, *et al* (2010) MTM1 mutation associated with X-linked myotubular myopathy in Labrador Retrievers. Proc Natl Acad Sci USA 107: 14697-14702

Bergmeyer HU, Bernt E (1974) Determination of glucose with glucose oxidase and peroxidase. *In Methods of Enzymatic Analysis*, pp 1205-1215. Weinheim-London: Verlag Chemie-Academic Press

Byfield MP, Murray JT, Backer JM (2005) hVps34 is a nutrient-regulated lipid kinase required for activation of p70 S6 kinase. J Biol Chem 280: 33076-33082

Chen D, Fan W, Lu Y, Ding X, Chen S, Zhong Q (2012) A mammalian autophagosome maturation mechanism mediated by TECPR1 and the Atg12-Atg5 conjugate. Mol Cell 45: 629-641

Codogno P, Mehrpour M, Proikas-Cezanne T (2011) Canonical and non-canonical autophagy: variations on a common theme of self-eating? Nat Rev Mol Cell Biol 13: 7-12

Dennis PB, Mercer CA (2009) The GST-BHMT assay and related assays for autophagy. Methods Enzymol 452: 97-118

Duran A, Amanchy R, Linares JF, Joshi J, Abu-Baker S, Porollo A, Hansen M, Moscat J, Diaz-Meco MT (2011) p62 is a key regulator of nutrient sensing in the mTORC1 pathway. Mol Cell 44: 134-146

Eskelinen EL, Illert AL, Tanaka Y, Schwarzmann G, Blanz J, von Figura K, Saftig P (2002) Role of LAMP-2 in lysosome biogenesis and autophagy. Mol Biol Cell 13: 3355-3368

Eskelinen EL, Saftig P (2009) Autophagy: a lysosomal degradation pathway with a central role in health and disease. Biochim Biophys Acta 1793: 664-673

Fuller M, Meikle PJ, Hopwood JJ (2006) Epidemiology of lysosomal storage diseases: an overview. In *Fabry Disease: Perspectives from 5 Years of FOS*, Mehta A, Beck M, Sunder-Plassmann G (Eds) Oxford: Oxford PharmaGenesis, Chapter 2

Gaullier JM, Ronning E, Gillooly DJ, Stenmark H (2000) Interaction of the EEA1 FYVE finger with phosphatidylinositol 3-phosphate and early endosomes. Role of conserved residues. J Biol Chem 275: 24595-24600

Grumati P, Coletto L, Sabatelli P, Cescon M, Angelin A, Bertaggia E, Blaauw B, Urciuolo A, Tiepolo T, Merlini L, *et al* (2010) Autophagy is defective in collagen VI muscular dystrophies, and its reactivation rescues myofiber degeneration. Nat Med 16: 1313-1320

Hariharan N, Maejima Y, Nakae J, Paik J, Depinho RA, Sadoshima J (2010) Deacetylation of FoxO by Sirt1 plays an essential role in mediating starvation-induced autophagy in cardiac myocytes. Circ Res 107: 1470-1482

Head SI, Williams DA, Stephenson DG (1992) Abnormalities in structure and function of limb skeletal muscle fibres of dystrophic mdx mice. Proc Biol Sci 248: 163-169

Jaber N, Dou Z, Chen JS, Catanzaro J, Jiang YP, Ballou LM, Selinger E, Ouyang X, Lin RZ, Zhang J, *et al* (2012) Class III PI3K Vps34 plays an essential role in autophagy and in heart and liver function. Proc Natl Acad Sci USA 109: 2003-2008

Juhasz G, Hill JH, Yan Y, Sass M, Baehrecke EH, Backer JM, Neufeld TP (2008) The class III PI(3)K Vps34 promotes autophagy and endocytosis but not TOR signaling in Drosophila. J Cell Biol 181: 655-666

Jung CH, Ro SH, Cao J, Otto NM, Kim DH (2010) mTOR regulation of autophagy. FEBS Lett 584: 1287-1295

Kihara A, Noda T, Ishihara N, Ohsumi Y (2001) Two distinct Vps34 phosphatidylinositol 3-kinase complexes function in autophagy and carboxypeptidase Y sorting in Saccharomyces cerevisiae. J Cell Biol 152: 519-530

Kimura S, Noda T, Yoshimori T (2007) Dissection of the autophagosome maturation process by a novel reporter protein, tandem fluorescent-tagged LC3. Autophagy 3: 452-460

Klionsky DJ (2007) Autophagy: from phenomenology to molecular understanding in less than a decade. Nat Rev Mol Cell Biol 8: 931-937

Komatsu M, Waguri S, Ueno T, Iwata J, Murata S, Tanida I, Ezaki J, Mizushima N, Ohsumi Y, Uchiyama Y, *et al* (2005) Impairment of starvation-induced and constitutive autophagy in Atg7-deficient mice. J Cell Biol 169: 425-434

Kuma A, Hatano M, Matsui M, Yamamoto A, Nakaya H, Yoshimori T, Ohsumi Y, Tokuhisa T, Mizushima N (2004) The role of autophagy during the early neonatal starvation period. Nature 432: 1032-1036

Lee JA, Beigneux A, Ahmad ST, Young SG, Gao FB (2007) ESCRT-III dysfunction causes autophagosome accumulation and neurodegeneration. Curr Biol 17: 1561-1567

Lee JA, Gao FB (2009) Inhibition of autophagy induction delays neuronal cell loss caused by dysfunctional ESCRT-III in frontotemporal dementia. J Neurosci 29: 8506-8511

Malicdan MC, Noguchi S, Nonaka I, Saftig P, Nishino I (2008) Lysosomal myopathies: an excessive build-up in autophagosomes is too much to handle. Neuromuscul Disord 18: 521-529

Mammucari C, Milan G, Romanello V, Masiero E, Rudolf R, Del Piccolo P, Burden SJ, Di Lisi R, Sandri C, Zhao J, *et al* (2007) FoxO3 controls autophagy in skeletal muscle in vivo. Cell Metab 6: 458-471

Masiero E, Agatea L, Mammucari C, Blaauw B, Loro E, Komatsu M, Metzger D, Reggiani C, Schiaffino S, Sandri M (2009) Autophagy is required to maintain muscle mass. Cell Metab 10: 507-515

Matsunaga K, Saitoh T, Tabata K, Omori H, Satoh T, Kurotori N, Maejima I, Shirahama-Noda K, Ichimura T, Isobe T, *et al* (2009) Two Beclin 1-binding proteins, Atg14L and Rubicon, reciprocally regulate autophagy at different stages. Nat Cell Biol 11: 385-396

McLeod IX, Zhou X, Li QJ, Wang F, He YW (2011) The class III kinase Vps34 promotes T lymphocyte survival through regulating IL-7Ralpha surface expression. J Immunol 187: 5051-5061

Mehrpour M, Esclatine A, Beau I, Codogno P (2010) Overview of macroautophagy regulation in mammalian cells. Cell Res 20: 748-762

Mercer CA, Kaliappan A, Dennis PB (2008) Macroautophagy-dependent, intralysosomal cleavage of a betaine homocysteine methyltransferase fusion protein requires stable multimerization. Autophagy 4: 185-194

Miniou P, Tiziano D, Frugier T, Roblot N, Le Meur M, Melki J (1999) Gene targeting restricted to mouse striated muscle lineage. Nucleic Acids Res 27: e27

Mizushima N, Yamamoto A, Matsui M, Yoshimori T, Ohsumi Y (2004) in vivo analysis of autophagy in response to nutrient starvation using transgenic mice expressing a fluorescent autophagosome marker. Mol Biol Cell 15: 1101-1111

Nishino I (2003) Autophagic vacuolar myopathies. Curr Neurol Neurosci Rep 3: 64-69

Nishino I, Fu J, Tanji K, Yamada T, Shimojo S, Koori T, Mora M, Riggs JE, Oh SJ, Koga Y, *et al* (2000) Primary LAMP-2 deficiency causes X-linked vacuolar cardiomyopathy and myopathy (Danon disease). Nature 406: 906-910

Nobukuni T, Joaquin M, Roccio M, Dann SG, Kim SY, Gulati P, Byfield MP, Backer JM, Natt F, Bos JL, *et al* (2005) Amino acids mediate mTOR/raptor signaling through activation of class 3 phosphatidylinositol 3OH-kinase. Proc Natl Acad Sci USA 102: 14238-14243

Pena-Llopis S, Vega-Rubin-de-Celis S, Schwartz JC, Wolff NC, Tran TA, Zou L, Xie XJ, Corey DR, Brugarolas J (2011) Regulation of TFEB and V-ATPases by mTORC1. EMBO J 30: 3242-3258

Proikas-Cezanne T, Pfisterer SG (2009) Assessing mammalian autophagy by WIPI-1/Atg18 puncta formation. Methods Enzymol 452: 247-260

Proikas-Cezanne T, Ruckerbauer S, Stierhof YD, Berg C, Nordheim A (2007) Human WIPI-1 puncta-formation: a novel assay to assess mammalian autophagy. FEBS Lett 581: 3396-3404

Proikas-Cezanne T, Waddell S, Gaugel A, Frickey T, Lupas A, Nordheim A (2004) WIPI-1alpha (WIPI49), a member of the novel 7-bladed WIPI protein family, is aberrantly expressed in human cancer and is linked to starvation-induced autophagy. Oncogene 23: 9314-9325

Raben N, Hill V, Shea L, Takikita S, Baum R, Mizushima N, Ralston E, Plotz P (2008) Suppression of autophagy in skeletal muscle uncovers the accumulation of ubiquitinated proteins and their potential role in muscle damage in Pompe disease. Hum Mol Genet 17: 3897-3908

Raben N, Schreiner C, Baum R, Takikita S, Xu S, Xie T, Myerowitz R, Komatsu M, Van der Meulen JH, Nagaraju K, *et al* (2010) Suppression of autophagy permits successful enzyme replacement therapy in a lysosomal storage disorder–murine Pompe disease. Autophagy 6: 1078-1089

Robinson JS, Klionsky DJ, Banta LM, Emr SD (1988) Protein sorting in Saccharomyces cerevisiae: isolation of mutants defective in the delivery and processing of multiple vacuolar hydrolases. Mol Cell Biol 8: 4936-4948

Rusten TE, Stenmark H (2010) p62, an autophagy hero or culprit? Nat Cell Biol 12: 207-209

Rusten TE, Vaccari T, Lindmo K, Rodahl LM, Nezis IP, Sem-Jacobsen C, Wendler F, Vincent JP, Brech A, Bilder D, *et al* (2007) ESCRTs and Fab1 regulate distinct steps of autophagy. Curr Biol 17: 1817-1825

Rusten TE, Vaccari T, Stenmark H (2012) Shaping development with ESCRTs. Nat Cell Biol 14: 38-45

Sandri M (2010) Autophagy in skeletal muscle. FEBS Lett 584: 1411-1416

Schu PV, Takegawa K, Fry MJ, Stack JH, Waterfield MD, Emr SD (1993) Phosphatidylinositol 3-kinase encoded by yeast VPS34 gene essential for protein sorting. Science 260: 88-91

Schwenk F, Baron U, Rajewsky K (1995) A cre-transgenic mouse strain for the ubiquitous deletion of loxP-flanked gene segments including deletion in germ cells. Nucleic Acids Res 23: 5080-5081

Shima H, Pende M, Chen Y, Fumagalli S, Thomas G, Kozma SC (1998) Disruption of the p70(s6k)/p85(s6k) gene reveals a small mouse phenotype and a new functional S6 kinase. EMBO J 17: 6649-6659

Simonsen A, Tooze SA (2009) Coordination of membrane events during autophagy by multiple class III PI3-kinase complexes. J Cell Biol 186: 773-782

Stenmark H, Aasland R (1999) FYVE-finger proteins–effectors of an inositol lipid. J Cell Sci 112: 4175-4183

Taguchi-Atarashi N, Hamasaki M, Matsunaga K, Omori H, Ktistakis NT, Yoshimori T, Noda T (2010) Modulation of local PtdIns3P levels by the PI phosphatase MTMR3 regulates constitutive autophagy. Traffic 11: 468-478

Tanaka Y, Guhde G, Suter A, Eskelinen EL, Hartmann D, Lullmann-Rauch R, Janssen PM, Blanz J, von Figura K, Saftig P (2000) Accumulation of autophagic vacuoles and cardiomyopathy in LAMP-2-deficient mice. Nature 406: 902-906

Thoresen SB, Pedersen NM, Liestol K, Stenmark H (2010) A phosphatidylinositol 3-kinase class III sub-complex containing VPS15, VPS34, Beclin 1, UVRAG and BIF-1 regulates cytokinesis and degradative endocytic traffic. Exp Cell Res 316: 3368-3378

Vanhaesebroeck B, Guillermet-Guibert J, Graupera M, Bilanges B (2010) The emerging mechanisms of isoform-specific PI3K signalling. Nat Rev Mol Cell Biol 11: 329-341

Vergne I, Deretic V (2010) The role of PI3P phosphatases in the regulation of autophagy. FEBS Lett 584: 1313-1318

Willinger T, Flavell RA (2012) Canonical autophagy dependent on the class III phosphoinositide-3 kinase Vps34 is required for naive T-cell homeostasis. Proc Natl Acad Sci USA 109: 8670-8675

Yan Y, Flinn RJ, Wu H, Schnur RS, Backer JM (2009) hVps15, but not Ca2+/CaM, is required for the activity and regulation of hVps34 in mammalian cells. Biochem J 417: 747-755

Yoon MS, Du G, Backer JM, Frohman MA, Chen J (2011) Class III PI-3-kinase activates phospholipase D in an amino acid-sensing mTORC1 pathway. J Cell Biol 195: 435-447

Zhong Y, Wang QJ, Li X, Yan Y, Backer JM, Chait BT, Heintz N, Yue Z (2009) Distinct regulation of autophagic activity by Atg14L and Rubicon associated with Beclin 1-phosphatidylinositol-3-kinase complex. Nat Cell Biol 11: 468-476

Zhou X, Takatoh J, Wang F (2011) The mammalian class 3 PI3K (PIK3C3) is required for early embryogenesis and cell proliferation. PLoS One 6: e16358

Zoncu R, Bar-Peled L, Efeyan A, Wang S, Sancak Y, Sabatini DM (2011) mTORC1 senses lysosomal amino acids through an inside-out mechanism that requires the vacuolar H-ATPase. Science 334: 678-683

Neuropathology and Applied Neurobiology (2013), **39**, 449–453 doi: 10.1111/nan.12018

Scientific correspondence

Juvenile autophagic vacuolar myopathy – a new entity or variant?

Autophagic vacuolar myopathies (AVMs) comprise a heterogeneous cluster of diseases. These include lysosomal storage disease with or without abnormal acid maltase activity such as glycogen storage disease (GSD) type II (OMIM 232300) and lysosomal membrane protein LAMP-2-deficient Danon disease (OMIM 300257) [1] caused by mutations in the *LAMP-2* gene (OMIM 309060). X-linked myopathy with excessive autophagy (XMEA; OMIM 310440), infantile AVM (OMIM 609500) and adult onset AVM with multi-organ involvement are also included in the spectrum of AVMs [2–5]. These latter diseases demonstrate distinct pathomorphological features, including vacuoles with autophagy-associated proteins and immunoreactivity for a multitude of sarcolemmal proteins (e.g. dystrophin, β-spectrin, dysferlin, caveolin-3, sarcoglycans), prominent acetylcholine esterase (AChE) activity and complement deposition [3,6]. Particularly in XMEA, ultrastructural evidence of intravacuolar debris associated with multiplication of the basal lamina and fusion of the vacuoles with the sarcolemma have been described as specific hallmarks for the disease, suggesting an aberrant exocytotic process [2,6]. Furthermore, the *VMA21* gene on chromosome Xq28, which encodes a chaperone for assembly of lysosomal vacuolar ATPase, has been established as responsible for XMEA [7]. It is likely that AVMs share a common pathomechanism related to a dysfunctional autophagosomal machinery [1,6].

After a normal post-natal and infantile development, a 14-year-old boy from Yemen presented with mild proximal weakness affecting his lower extremities for a duration of 1 year. He showed Gowers sign upon neurological examination. Strength in his arms and distal leg muscles was unremarkable as was the rest of the entire neurological examination. In particular, no evidence of muscle or tendon contractures was found. Creatine kinase was elevated up to 15-fold, and a cardiac work-up disclosed a Wolf-Parkinson-White syndrome by 24-h electrocardiography, but no signs of cardiomyopathy by echocardiography, and no involvement of further internal organs was detectable. He had no intellectual deficits, and his family history was reported to be unremarkable, notably with an absence of a history of muscle diseases.

A biopsy specimen from the quadriceps muscle was subjected to routine enzyme histochemistry, immunohistochemistry and ultrastructural examination. In most fibres, numerous vacuoles inside the sarcoplasm exhibited sarcolemmal lining, demonstrated by the strong but variable expression of plasma membrane- or basal lamina-associated proteins, including β-spectrin, caveolin-3, laminin-α2 (300 kDa) (Figure 1**B–D**), dystrophin and dysferlin (not shown). Interestingly, invagination of the sarcolemma could be detected in Gomori trichrome, β-spectrin, caveolin 3, laminin-α2 and major histocompatibility complex (MHC) class I stains (Figure 1**A–D**, **F**). Vacuoles contained both AChE (Figure 2**A**) and non-specific esterase (Figure 2**C**) but lacked acid phosphatase activity (Figure 2**B**). Vacuoles were also lined by complement (C5b9), but none of the fibres demonstrated C5b9 staining of the sarcolemma (Figure 1**E**). Furthermore, MHC class I was upregulated on the sarcolemma and on the vacuolar lining (Figure 1**F**), while neither stained for MHC class II (not shown). Large autophagosomes were strongly immunopositive for LC3 (Figure 2**D**). Interestingly, LAMP-2 was strongly positive on numerous lysosomes (Figure 2**E**), which were more densely packed and larger when compared to normal controls (Figure 2**E**, inset). Ultrastructural studies identified cellular debris and myelin-like features in the centre of vacuoles (Figure 2**F**) as well as duplicated basal laminae (Figure 2**G**) and accumulation of glycogen, which was not membrane-bound (Figure 2**H**). Fusion of vacuoles with the sarcolemma of muscle fibres was not a detectable feature of this biopsy specimen.

Molecular sequencing was performed and ruled out GSD II (juvenile 'Pompe' disease), Danon disease and XMEA. Sequencing of the entire *GAA* gene on chromosome 17q25, *LAMP-2* gene on chromosome Xq24 as well as the *VMA21* gene on chromosome Xq28 failed to reveal deletions.

Taken together, the present case may represent the manifestation of a new disease or a variant among the genetically unidentified congenital infantile and adult AVM displaying some similarities with XMEA, but also distinctive clinicopathological features. We describe a juvenile male subject with normal intelligence suffering

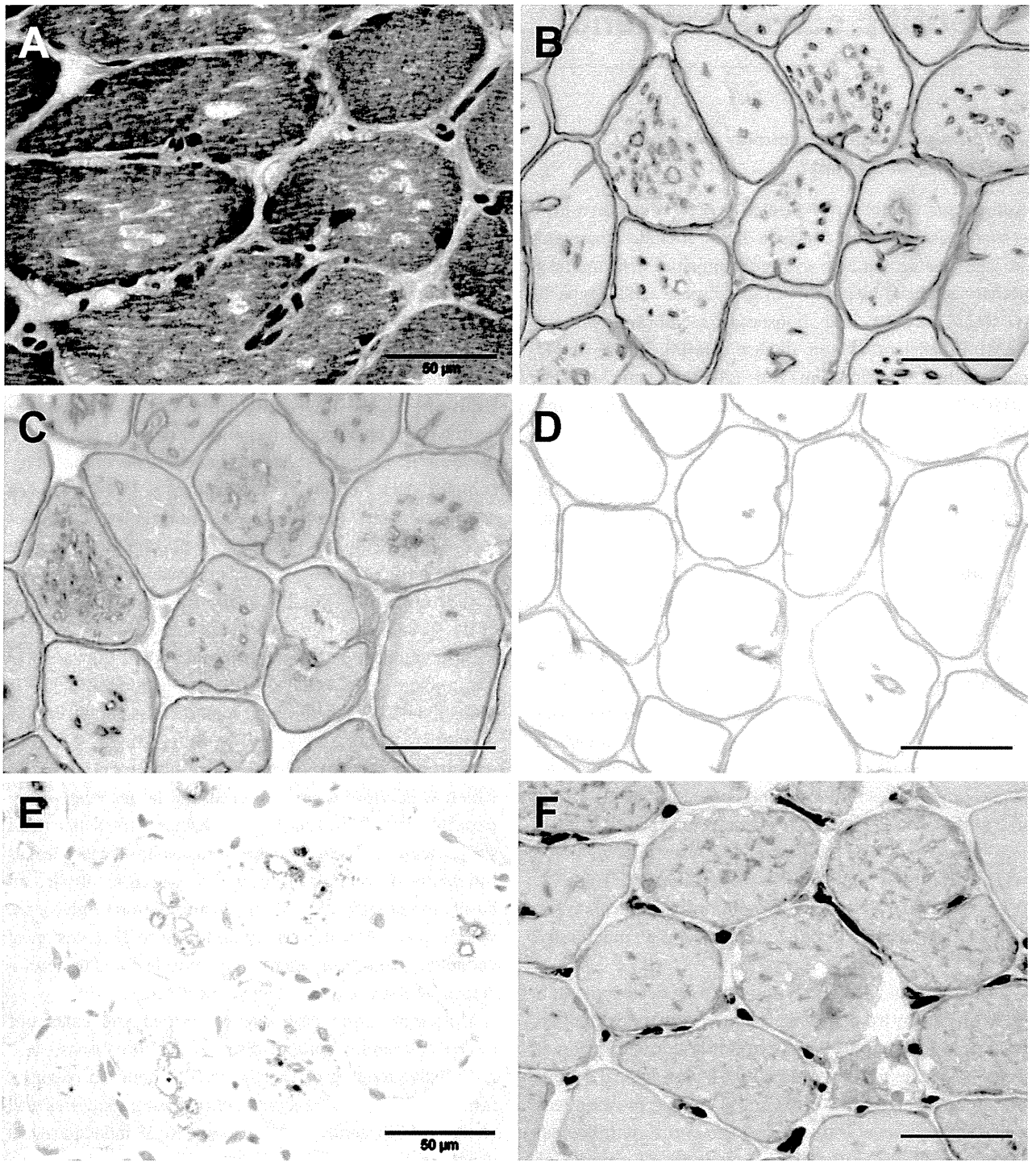

Figure 1. Myopathological characteristics of juvenile autophagic vacuolar myopathy with sarcolemmal features. Numerous vacuoles are illustrated by a Gomori trichrome stain in nearly every muscle fibre (**A**). Sarcolemmal features with lining of the vacuoles by sarcolemmal and basal lamina proteins at varying intensity are exemplified by β-spectrin (**B**), caveolin-3 (**C**) and laminin-α2 (300 kDa) stains (**D**). Complement deposition of the membrane attack complex (C5b9) was strongly positive in the vacuoles and in the vacuolar lining but negative on the sarcolemma of muscle fibres (**E**), while major histocompatibility complex class I is found on the vacuolar lining and on the sarcolemma (**F**).

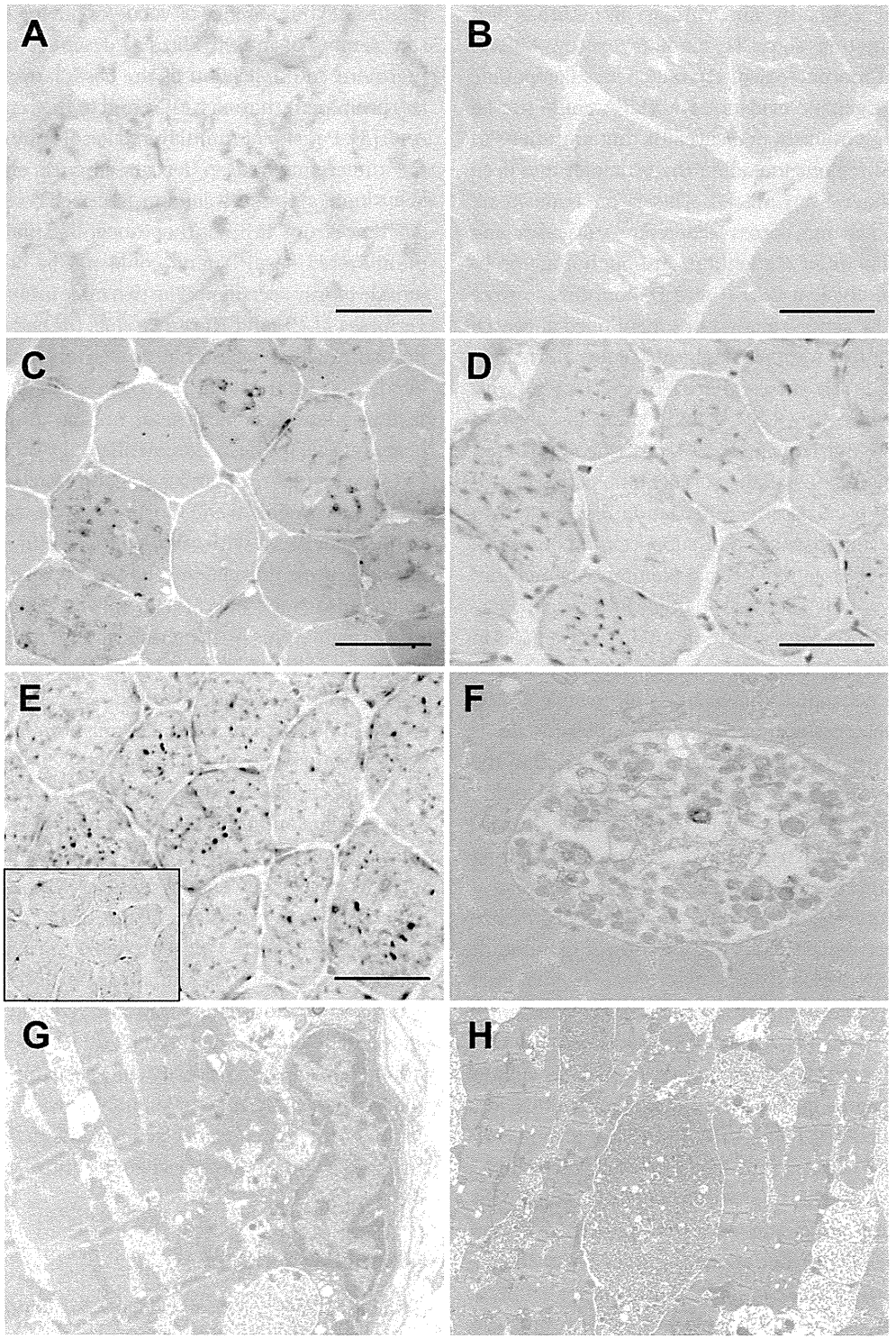

Figure 2. Light microscopic and ultrastructural characteristics of juvenile autophagic vacuolar myopathy with sarcolemmal features. The content of most vacuoles is positive for acetylcholine esterase (**A**), negative for acid phosphatase (**B**) but positive for non-specific esterase (**C**). Autophagic activity of large lysosomes is documented by LC3 immunostaining (**D**). Strong immunoreactivity of LAMP-2 protein is identified on these large lysosomes (**E**). The inset shows a healthy control muscle, with smaller lysosomes. Ultrastructural analysis reveals cellular debris, myelin-like formations and glycogen in vacuoles (**F**). Additionally duplicated basal laminae are illustrated (**G**), but exocytosed material between them is absent. Intermyofibrillar accumulation of glycogen which is not membrane-bound is illustrated (**H**).

from proximal myopathy and cardiac arrhythmia, but without manifesting signs of cardiomyopathy. Muscle biopsy showed morphological characteristics compatible with AVM, but genetic evidence for XMEA could not be found. Although unlikely, one caveat is that mutations in non-sequenced regions including the promoter and deep introns may have been missed. This is an issue in all sequencing endeavours across all hereditary diseases, and thus a general point of contention. Although not a probable diagnosis, atypical GSD II and Danon disease were also ruled out by genetic analyses as mentioned above. Of note, some features were particularly unique to the case and of diagnostic relevance; others were overlapping with details found in XMEA, GSD II and Danon disease and in the twin girls harbouring AVMs, described by Holton *et al.* [5]. Invaginations of the sarcolemma as illustrated here have also been described in Danon disease and in the report by Holton *et al.*, and support the concept of autophagosomal isolation of sarcolemmal membranes prior to fusion with lysosomes [1]. Importantly, acid phosphatase activity was consistently absent in the vacuoles in this juvenile patient's muscle tissue, which is known to be very strong in lysosomes and vacuoles of juvenile GSD II patients' muscle tissues. Further, acid phosphatase is present but less pronounced in Danon disease and in the twin girls' muscles reported by Holton *et al.*, while strong acid phosphatase positivity was reported in a Chinese patient's muscle who was one of seven affected boys suffering from congenital X-linked AVM [4]. Excessive LAMP-2 immunoreactivity on lysosomal structures has thus far not been described in infantile cases or in the adult case of AVM [4,8–11], but it was described to be increased in the report by Yan *et al.* in the patient of the congenital X-linked AVM family [4]. LAMP-2 immunoreactivity was not tested in the report on twin girls with AVM by Holton *et al.*, but mutations in the corresponding gene have formally been ruled out [5]. LAMP-2 staining in our case illustrates unusually large autophagosomes, which can be detected by the LC3 stain as well. Absence of complement deposition on the sarcolemma but strong presence on the vacuolar lining is a further relevant immunohistochemical feature of our patient's muscle tissue, presented here. The twin girls described by Holton *et al.* [5], and the patient from the family of congenital X-linked AVM [4], exhibited both sarcolemmal and vacuolar staining of complement. Finally, the ultrastructural morphology differs from the classical morphology of XMEA. We provide evidence of vacuoles containing cellular debris (Figure 2**F**) but absence of vacuoles having fused with the sarcolemma of muscle fibres as described in XMEA. Furthermore, multiplication of the basal lamina was clearly less prominent than in XMEA and in the report by Holton *et al.* [5]. Paucity of multilayered basal lamina may also be the underlying reason for an absence of complement deposition on the sarcolemma described here. Yet, another difference from XMEA is that exocytosed material between multilayered basal lamina could not be detected in our muscle biopsy specimen. The two male infants reported by Verloes *et al.* [9] and Morisawa *et al.* [8] had severe cardiomyopathy, which was lethal, as well as generalized muscle hypotonia. Interestingly, glycogen content was reported severely increased in skeletal muscle and especially in heart muscle in these aforementioned studies.

Taken together, a number of features in the present case are at variance with the morphology described in XMEA or the other AVMs with sarcolemmal features published to date. Further, the patient showed cardiac involvement, which also does not fit clinically with XMEA, where cardiac symptoms are generally absent. One example that contradicts this observation is a report of two male siblings with the severe congenital form of XMEA, one of whom suffered from cardiac right bundle branch block and left ventricular hypertrophy, while his brother did not show any cardiac involvement [4].

In conclusion, our 14-year-old patient is the first juvenile male subject reported with a proximal myopathy due to AVM with sarcolemmal features. Genetically, XMEA, which is due to mutations of the *VMA21* gene on chromosome Xq28, as the most probable cause was ruled out. Although very rare, it is important to consider AVM and thus perform muscle biopsy and appropriate analysis including electron microscopy to improve our understanding of the morphological spectrum of AVM. We believe that modern genetic analysis will lead to identification of further causative genes and functional concepts for these obviously heterogeneous entities grouped under the term AVM.

Acknowledgement

Gina D. Eom is acknowledged for kindly reviewing grammar and style of the text.

Authors' contributions

Drs Werner Stenzel, Ichizo Nishino and Hans-Hilmar Goebel drafted and revised the manuscript, designed the

study concept, did the analysis and participated in the acquisition of data. Drs Arpad von Moers and Frank L. Heppner helped in drafting and revising the manuscript, did the analysis of data and participated in the acquisition of data. Drs Dieter Glaeser and Mahdi A. Kadry did the analysis of data and participated in the acquisition of data.

W. Stenzel*
I. Nishino**
A. von Moers†
M. A. Kadry‡
D. Glaeser§
F. L. Heppner*
H.-H. Goebel*¶

**Department of Neuropathology, Charité – Universitätsmedizin Berlin, †Department of Pediatrics and Neuropaediatrics, DRK Klinikum Westend, Berlin, ‡Department of Surgery and Vascular Surgery, KGM Klinikum Pritzwalk, Pritzwalk, §Genetikum Neu-Ulm, Ulm, ¶Department of Neuropathology, University Medicine, Johannes Gutenberg University, Mainz, Germany, and **National Institute of Neuroscience, National Center of Neurology and Psychiatry, Tokyo, Japan*

References

1 Malicdan MC, Nishino I. Autophagy in lysosomal myopathies. *Brain Pathol* 2012; **22**: 82–8
2 Nishino I. Autophagic vacuolar myopathy. *Semin Pediatr Neurol* 2006; **13**: 90–5
3 Sugie K, Noguchi S, Kozuka Y, Arikawa-Hirasawa E, Tanaka M, Yan C, Saftig P, von Figura K, Hirano M, Ueno S, Nonaka I, Nishino I. Autophagic vacuoles with sarcolemmal features delineate Danon disease and related myopathies. *J Neuropathol Exp Neurol* 2005; **64**: 513–22
4 Yan C, Tanaka M, Sugie K, Nobutoki T, Woo M, Murase N, Higuchi Y, Noguchi S, Nonaka I, Hayashi YK, Nishino I. A new congenital form of X-linked autophagic vacuolar myopathy. *Neurology* 2005; **65**: 1132–4
5 Holton JL, Beesley C, Jackson M, Venner K, Bhardwaj N, Winchester B, Al-Memar A. Autophagic vacuolar myopathy in twin girls. *Neuropathol Appl Neurobiol* 2006; **32**: 253–9
6 Malicdan MC, Noguchi S, Nonaka I, Saftig P, Nishino I. Lysosomal myopathies: an excessive build-up in autophagosomes is too much to handle. *Neuromuscul Disord* 2008; **18**: 521–9
7 Ramachandran N, Munteanu I, Wang P, Ruggieri A, Rilstone JJ, Israelian N, Naranian T, Paroutis P, Guo R, Ren ZP, Nishino I, Chabrol B, Pellissier J-F, Minetti C, Udd B, Fardeau M, Tailor CS, Mahuran DJ, Kissel JT, Kalimo H, Levy N, Manolson MF, Ackerley CA, Minassian BA. VMA21 deficiency prevents vacuolar ATPase assembly and causes autophagic vacuolar myopathy. *Acta Neuropathologica* 2013, in press (doi 10.1007/s00401-012-1073-6)
8 Morisawa Y, Fujieda M, Murakami N, Naruse K, Okada T, Morita H, Sawada K, Miyazaki J, Kurashige T, Nonaka I. Lysosomal glycogen storage disease with normal acid maltase with early fatal outcome. *J Neurol Sci* 1998; **160**: 175–9
9 Verloes A, Massin M, Lombet J, Grattagliano B, Soyeur D, Rigo J, Koulischer L, Van Hoof F. Nosology of lysosomal glycogen storage diseases without in vitro acid maltase deficiency. Delineation of a neonatal form. *Am J Med Genet* 1997; **72**: 135–42
10 Yamamoto A, Morisawa Y, Verloes A, Murakami N, Hirano M, Nonaka I, Nishino I. Infantile autophagic vacuolar myopathy is distinct from Danon disease. *Neurology* 2001; **57**: 903–5
11 Kaneda D, Sugie K, Yamamoto A, Matsumoto H, Kato T, Nonaka I, Nishino I. A novel form of autophagic vacuolar myopathy with late-onset and multiorgan involvement. *Neurology* 2003; **61**: 128–31

Received 3 August 2012
Accepted after revision 7 January 2013
Published online Article Accepted on 7 January 2013

V. 研 究 者 一 覧

遠位型ミオパチーにおけるN-アセチルノイラミン酸の薬物動態の検討及び第2/3相試験

研究代表者	青木　正志	東北大学大学院医学系研究科　神経内科学
研究分担者	西野　一三	国立精神・神経医療研究センター神経研究所疾病研究第一部
	島崎　茂樹	ノーベルファーマ株式会社、医薬品開発　研究開発本部
	割田　仁	東北大学大学院医学系研究科　神経内科学
	加藤　昌昭	東北大学病院　神経内科
事務局	加藤　昌昭	東北大学 神経内科
	武藤久美子	東北大学 神経内科